



Facile non-pressurized synthesis of nanowire-constructed hierarchical TiO₂ nanomaterials with improved dye sensitized solar cell performance

Yinghao Lv¹ · Rui Zan¹ · Xiaogang Wen¹

Received: 10 January 2019 / Accepted: 26 June 2019 / Published online: 2 July 2019
© Springer Science+Business Media, LLC, part of Springer Nature 2019

Abstract

Nanowire-constructed hierarchical TiO₂ nanomaterials (HTN) are prepared by a facile non-hydrothermal method at atmospheric pressure. The product is characterized in detail using powder X-ray diffraction, scanning electron microscopy, transmission electron microscopy and UV–Vis spectrophotometer. The synthesized TiO₂ hierarchical nanomaterials consist of nanowires of 15 nm in diameter, it possesses a high surface area of 144.65 m²/g, and demonstrate an excellent dye absorption ability (155.55 nmol/cm²), which is 2.7 times more than that of the Degussa P25. Corresponding photovoltaic performance of dye-sensitized solar cells (DSSCs) fabricated from HTN is also investigated. It exhibits an overall light-to-electricity conversion efficiency of 8.9% accompanying a short-circuit current density of 20.43 mA/cm², an open-circuit voltage of 720 mV and fill factor of 0.61, which is much higher than that of P25 (5.5%). The significant enhancement of short-circuit current density and power conversion efficiency of HTN can be attributed to its larger dye loading amount, better charge transportation ability and excellent light scattering ability.

1 Introduction

Solar cells are environment-friendly and renewable power source devices, which have potential for fulfilling future energy demands in our world. Among various solar cells, dye-sensitized solar cells (DSSCs) attract an extensive attention owing to their low production cost, high efficiency, green production process and simple fabrication [1, 2]. Titanium dioxide (TiO₂) is the most promising candidate for photo-anode material in DSSCs due to its low cost, long-term stability and the best comprehensive performance [3]. Besides, TiO₂ nanomaterials have also been applied in Li ion battery [4–6], photocatalysis [7–10] etc. extensively.

The size, morphology and microstructure of nanomaterials have a great effect on its performance, the hierarchical TiO₂ nanomaterials consisting of one dimensional

(1D) nanounits demonstrated much improved DSSCs performance, which can be attributed to their excellent dye adsorption, light scattering and charge transportation ability. Various TiO₂ 1D nanomaterials including nanowires [11, 12], nanofibers [13], nanorods [14–16], nanotubes [17–20], 1D nanomaterials-constructed hierarchical nanoflowers [16, 21, 22] and microspheres [23–25] etc. have been synthesized successfully. Up to now, 1D TiO₂ nanomaterials have been mainly synthesized via hydrothermal, electrospinning or electrochemical anodic oxidation methods, especially, TiO₂ 1D nanomaterials with good crystallization were usually obtained via hydrothermal/solvothermal process [11, 12, 14, 15]. Most of above methods are high energy-consumption, meanwhile, they are difficult to realize commercial production. So, developing a facile method to obtain 1D TiO₂ nanomaterials with good performance is still a challenge. The non-pressurized solution-phase synthesis is easier to realize mass production than hydrothermal technique. Kasuga et al. and Ohsaki et al. ever reported the synthesis of short TiO₂ nanotubes via a chemical process at 110 °C [26, 27], and the obtained TiO₂ nanotubes exhibited a DSSCs conversion efficiency of 7.1% [27]. Can 1D TiO₂ nanomaterials be formed at lower temperature? Can we tune its size and morphology under non-hydrothermal condition? In this paper, we synthesized hierarchical TiO₂ nanomaterials consisting of

Electronic supplementary material The online version of this article (<https://doi.org/10.1007/s10854-019-01788-x>) contains supplementary material, which is available to authorized users.

✉ Xiaogang Wen
wenxg2001@163.com

¹ School of Materials Science and Engineering, Sichuan University, Chengdu 610065, People's Republic of China

nanowires at a lower temperature (100 °C) under an atmospheric pressure successfully, and the synthesized nanowires-constructed hierarchical TiO₂ nanomaterials exhibited a high DSSC conversion efficiency of 8.9% with a high short-circuit current density of 20.43 mAcm². It indicates the hierarchical TiO₂ nanomaterials with excellent performance can be obtained at lower temperature and an atmospheric pressure via a simple route.

2 Experimental

2.1 Materials

Commerical P25 was purchased from Degussa, sodium hydroxide (NaOH), hydrochloric acid (HCl), acetic acid (AcOH), ethylcellulose, terpineol absolute ethanol (C₂H₅OH, 99.7%), and distilled water were purchased from Chengdu Kelong. Iodide (I₂, 99%), 4-tertbutyridine (TBP), guanidinium thiocyanate (GNCS), 1-butyl-3-methylimidazolium iodide (BMII), acetonitrile, and valeronitrile were purchased from Sigma-Aldrich. The Ru dye and cis-di(thiocyanato)-bis (2,2'-bipyridyl-4,4'-dicarboxylate) ruthenium(II) (N719) were purchased from Dyesol. Fluorine doped SnO₂ conductive glass (FTO) with a sheet resistance of 10–15 Ω/sq was purchased from NSG. All the chemicals were used directly without further purification and modification.

2.2 Preparation of hierarchical TiO₂ nanomaterials

The hierarchical TiO₂ nanomaterials were prepared by a simple solution-phase reaction at atmospheric pressure. At first, 2 g P25 and 100 mL NaOH(10 M) aqueous solution were added in a 250-mL triangle flask, after magnetic stirring for 30 min, the flask was heated in an oil bath for different interval at 100 °C, the products were collected by centrifugation and washed with deionized (DI) water for three times, and then, they were immersed in 0.1 M HCl aqueous solution for 12 h. The precipitates were washed with DI water for three times again, and dried at 70 °C for 24 h. Finally, the white powder was calcined at 500 °C for 3 h in air. The samples obtained after 2, 6, 10 h reaction time were denoted as HTN2, HTN6, HTN10 respectively.

2.3 Fabrication of DSSCs

Firstly, synthesized TiO₂ powder (or P25) (0.5 g) and acetic acid (100 μL) were added into ethanol (40 mL) to prepare slurry, after stirring for 3 h and sonicating for 0.5 h, 0.1 g ethylcellulose and 3 mL terpineol were added into the slurry, the mixture was stirred for 3 h and sonicated for 0.5 h continuously. A viscous white TiO₂ paste was obtained by

evaporating the mixture at 100 °C for 1 h. Then, the paste was doctor-bladed on the FTO substrates, followed by drying at 70 °C for 5 min and sintering at 500 °C for 30 min. Next, the films were treated in 0.04 M TiCl₄ aqueous solution at 70 °C for 30 min and calcined at 500 °C for 30 min again. Secondly, the photo-anodes were immersed into 0.5 mM N719 solution in dark and kept for 24 h at room temperature. Afterwards, the photo-anodes were washed with ethanol and dried with a hair drier. Finally, the N719 dye sensitized TiO₂/FTO films were sandwiched with platinum counter electrode and electrolyte was injected between two electrodes. The electrolyte was composed of 0.7 M 1-butyl-3-methylimidazolium iodide (BMII), 0.03 M I₂, 0.1 M guanidinium thiocyanate (GSCN) and 0.5 M 4-tertbutylpyridine (TBP) in acetonitrile and valeronitrile (85:15 v/v) mixed solvent. The area of active layer was 0.25 cm².

2.4 Characterizations

The morphology and size of the synthesized materials were examined by scanning electron microscopy (SEM, JEOLS-3400N, JEOLS-4800N) and transmission electron microscopy (TEM, FEI Titan G2 60-300), powder X-ray diffractometry (XRD, Bruker AXS-D8 Advance) was used to determine the crystal phase. The Brunauer–Emmett–Teller (BET) surface areas of the samples were derived using an ASAP 2460 volumetric adsorption analyzer. UV–visible absorption data were measured by a UV–Vis spectrophotometer (Shimadzu UV1700, PE lambda 750). The current–voltage characteristics of the cell were obtained by applying external potential bias to the cell and the generated photocurrent was recorded using an electrochemical workstation (Chenhua, CHI 660E, China) under one sun AM 1.5 G (100 mW/cm²) illumination with a solar light simulator (Zolix Sirius-SS150). A 1000 W Xenon arc lamp (Zolix LHX150) served as a light source and its incident light intensity was calibrated with a NREL-calibrated Si solar cell equipped with an optical filter to approximate one sun light intensity before each measurement. Electrochemical impedance spectroscopy (EIS) measurements were carried on an electrochemical workstation (Chenhua, CHI 660E) and further fitted by the Z-view software.

3 Result and discussion

3.1 Morphology and structure characterization of HTN

Morphology of HTN synthesized via low-temperature chemical process was analyzed by SEM. As shown in Fig. 1, all the products grown for different time possess similar cotton-like morphology, the samples demonstrate rough surface and

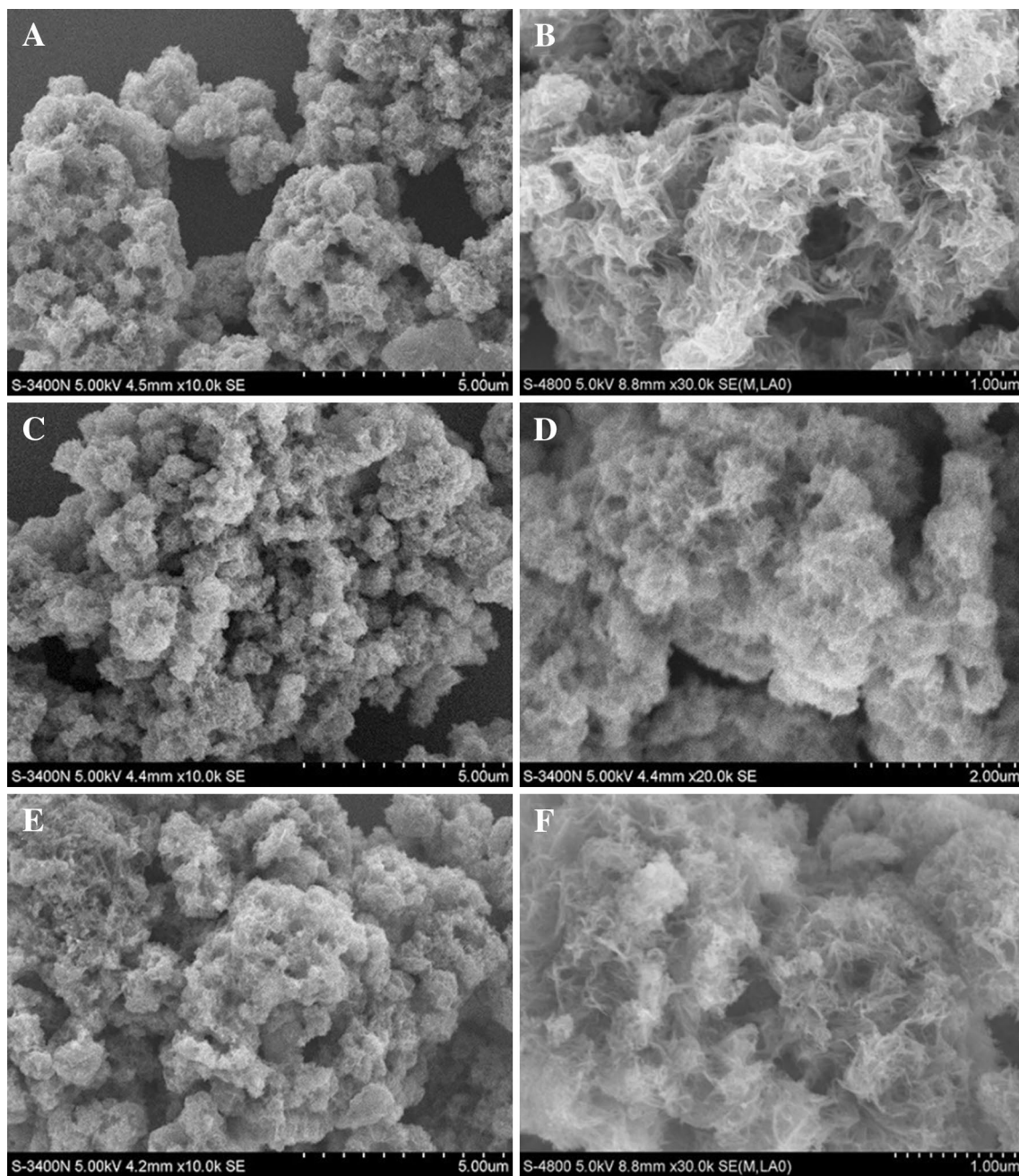


Fig. 1 SEM images with different magnification of HTN synthesized at different reaction time. **a, b** 2 h; **c, d** 6 h; **e, f** 10 h

aggregate together mostly, and its particles size are about 0.5–1 μm . Based on the SEM images with higher magnification (Fig. 1b, d, f), it is obvious that these cotton-like samples consisting of a lot of thin nanowires. The diameter of nanowires grown for different time are about 20–30 nm (2 h), 30–40 nm (6 h) and 30–50 nm (10 h) respectively, and with increasing reaction time, the nanowires have a trend of becoming longer and nonuniform.

Figure 2a, b show the TEM images of a typical sample (HTN2), it displays the microstructure of a single

microsphere-like HTN. It is clear that the HTN is constructed by numerous nanowires, the average diameter of nanowires is about 15 nm and all the nanowires tangle together. Figure 2c is the HRTEM image of several nanowires, the fringe spacing of 0.35 nm corresponding to the (101) planes of anatase TiO_2 . The SAED pattern of a single TiO_2 nanowire-microsphere is shown in Fig. 2d, indicating the polycrystalline characteristic of the HTN, the four main diffraction rings could be indexed to (101),

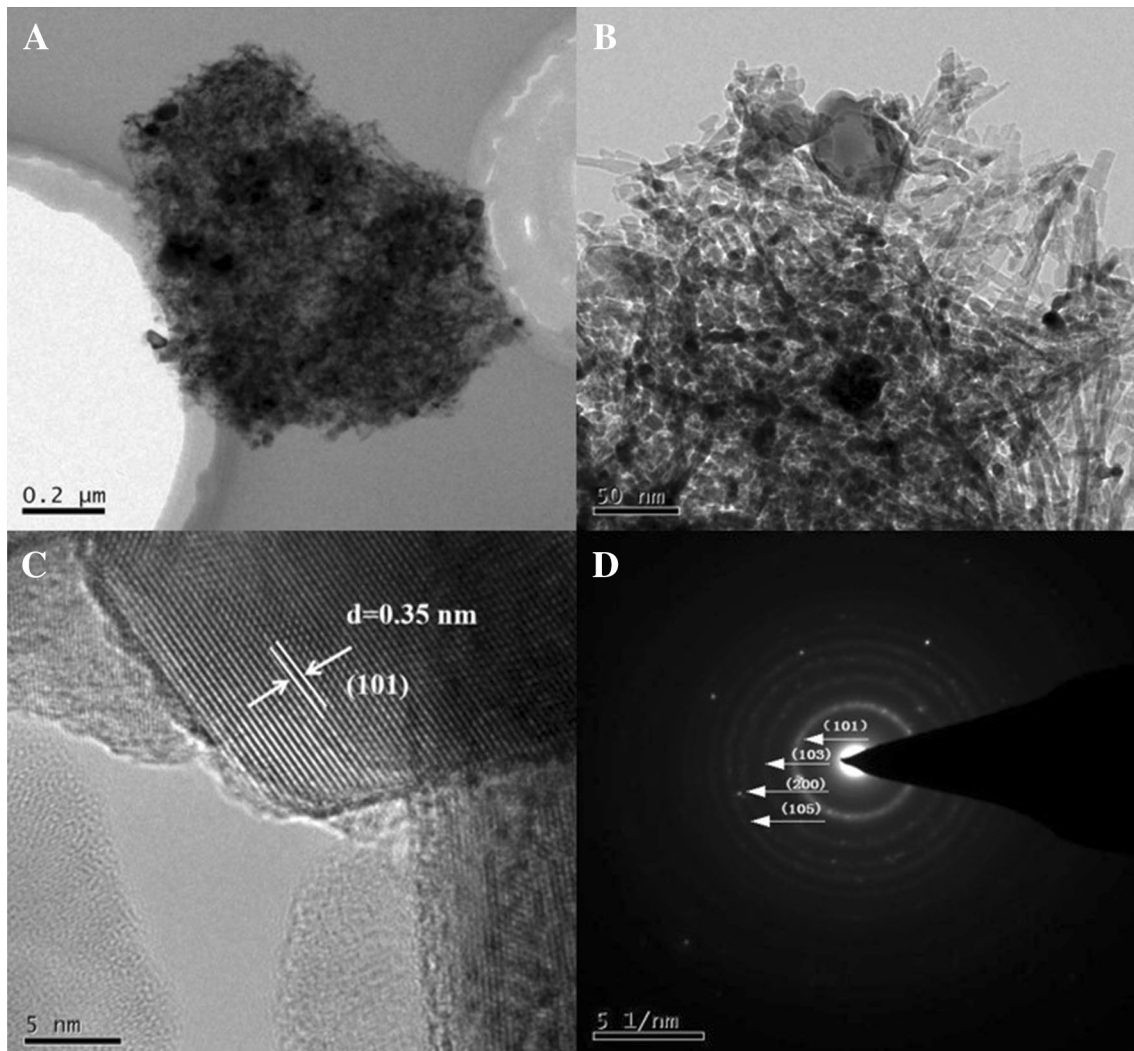


Fig. 2 **a** TEM images; **b** magnified TEM image; **c** HRTEM image; and **d** SAED pattern of sample HTN2 (grown for 2 h)

(103), (200) and (105) planes of the anatase TiO_2 , which are agreement with the following XRD analysis.

The powder XRD patterns of P25 and three samples prepared at different reaction time are shown in Fig. 3. It is clear that P25 contains anatase and rutile phase of TiO_2 . All three samples display same diffraction peaks at $2\theta = 25.3^\circ, 27.4^\circ, 36.1^\circ, 36.8^\circ, 37.8^\circ, 41.2^\circ, 48.1^\circ, 53.5^\circ, 54.3^\circ, 62.7^\circ, 69.1^\circ, 70.3^\circ$ and 75.2° , which correspond well to the (101), (103), (004), (200), (105), (204), (116), (220) and (215) lattice planes of anatase (JCPDS No. 21-1272) and (110), (101), (111), (211) lattice planes of rutile (JCPDS No. 21-1276) respectively, it indicates that the samples contain anatase and a little rutile phase. Based on the scherrer formula, the calculated crystallite size of HTN grown for 2 h, 6 h, 10 h are 10.8 nm, 13.9 nm, 16.9 nm respectively. It indicates that increasing reaction time promotes the further growth of TiO_2 nanocrystal, and induces the larger crystal size.

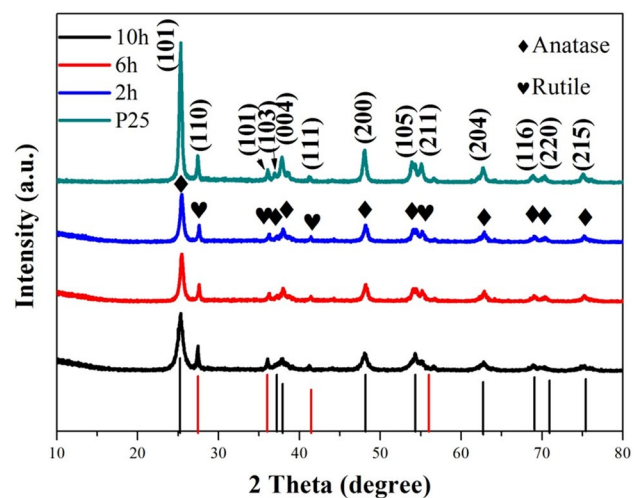


Fig. 3 XRD patterns of P25 and HTN synthesized at different reaction time

Figure 4 shows the adsorption–desorption isotherms of as-prepared HTN samples for different synthesis duration of 2 h, 6 h, 10 h, all three curves demonstrate a typical IUPAC type IV pattern [28], the calculated specific surface area is listed in Table 1, the specific surface area of 2 h, 6 h, 10 h sample are 144.65 m²/g, 121.72 m²/g, 86.58 m²/g respectively, suggesting that longer growth time will induce the rapid decrease of HTN surface area, which can be attributed the increased nanowire size (diameter and length). Inset of Fig. 4 demonstrates the pore size distribution of different samples, the total pore volumes of HTN2, HTN6, HTN10 are 0.89 cm³/g, 0.75 cm³/g, 0.37 cm³/g respectively, longer growth time will also induce smaller pore volume, which agrees with the increased nanowire diameter and density of HTN with longer reaction time. Due to specific surface area and pore ratio are directly related to the amount of dye adsorption, it implies that dye-adsorption ability will decrease accompanying increased growth time.

The performance of DSSCs fabricated from different samples and P25 was compared. Figure 5 shows the photocurrent density–voltage characteristics of cells with different photoanodes, and corresponding short-circuit current density (J_{SC}), open-circuit photo-voltage (V_{OC}), fill factor

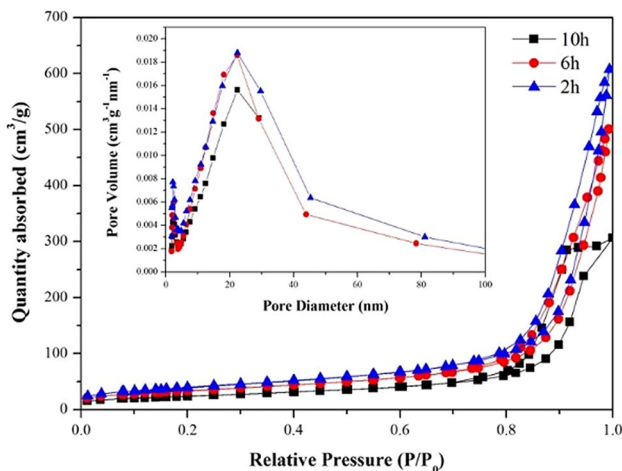


Fig. 4 Nitrogen adsorption–desorption isotherms of HTN synthesized at different reaction time. Inset: the pore size distribution of different samples

Table 1 The DSSC photovoltaic parameters, dye adsorption, surface area of different HTN and P25 samples

Cell (h)	J _{SC} (mA/cm ²)	V _{OC} (V)	FF	η (%)	Dye adsorption (nmol/cm ²)	Surface area (m ² /g)
HTN2	20.43	0.72	0.61	8.9	155.55	144.65
HTN6	14.74	0.73	0.69	7.4	132.16	121.72
HTN10	12.91	0.74	0.65	6.3	110.42	86.58
P25	12.04	0.79	0.57	5.46	57.60	54.42

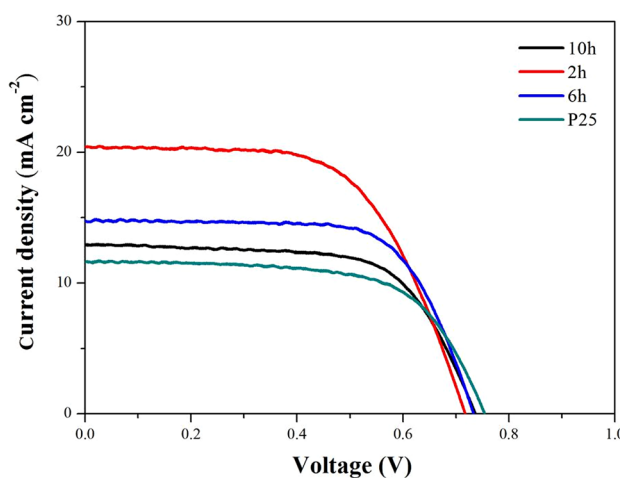


Fig. 5 Photocurrent density–voltage characteristics of 2 h, 6 h, 10 h HTN and P25 photoanodes under simulated AM 1.5 global sunlight (1 Sun, 100 mW cm⁻²)

(FF), overall conversion efficiency (η) of the cells, and dye adsorption amount and specific surface area are listed in Table 1. Among the investigated samples, HTN2 exhibits the best cell performance, presenting a J_{SC}, V_{OC}, FF, and cell efficiency of 20.43 mA/cm², 0.72 V, 0.61 and 8.9%, respectively. It is reasonably understood that HTN2 exhibits the highest cell efficiency due to it has largest surface area which is beneficial to adsorb more dye. For comparison, we also synthesized the sample with shorter growth time (1 h), the results are shown in Fig. S1. The samples grown for 1 h are nanoparticles, and it exhibits a conversion efficiency of 7%, which is lower than HTN2 and HTN6.

The amounts of dyes adsorbed on the photoanode films are obtained by measuring the UV–Vis absorption spectra of solutions containing dyes detached from the films (3 mL 0.1 M NaOH aqueous solution). Figure 6 shows the UV–Vis adsorption spectra of dye detached from different photoanodes, It is found that the dye amount on HTN2 film is obviously more than other films (Fig. 6; Table 1), this can be attributed to its higher surface area (Table 1), and it facilitates to produce more photo-generated electrons and obtain high photocurrents for the solar cell. We also measured the UV–Vis absorption spectra of HTN powder and

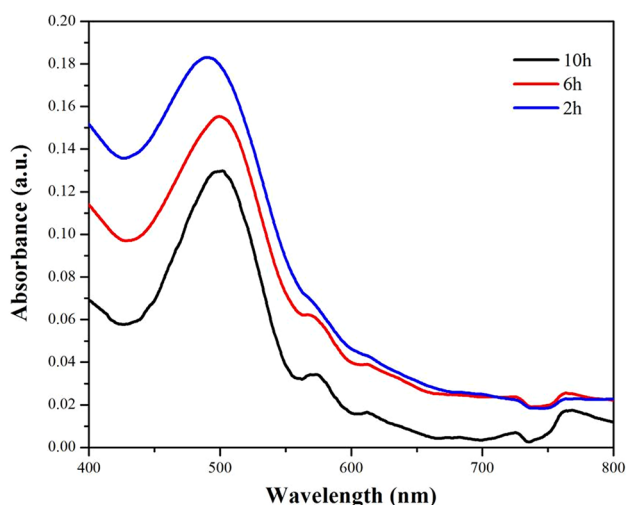


Fig. 6 UV-Vis absorption spectra of detached dye

dye loaded TiO₂ photoanode films, the results are shown in Fig. S2. It indicates that the visible light absorption of all the samples increase after dye loading, and HTN samples demonstrate stronger and wider absorption than P25 in visible light region.

Electrochemical impedance spectroscopy (EIS) is measured to further understand the electron transport and recombination process in the DSSCs based on the four different photoanodes. The Nyquist plots are exhibited in Fig. 7a and modeled with an equivalent circuit (inset of Fig. 7a) by using Z-view software. Table 2 lists the EIS parameters of the DSSCs based on the four different photoanodes. As shown in Fig. 7a, for all four photoanodes, a smaller semicircle at high frequency (1 kHz–1 MHz) and

Table 2 EIS parameters of the DSSCs based on the four different photoanodes

Sample	R1 (Ω)	R2 (Ω)	f_{\max} (Hz)	τ_r (ms)
HTN2	14.3	22.1	3.83	41.58
HTN6	20.1	28.3	12.1	13.16
HTN10	22.1	30.6	14.7	10.83
P25	20.9	46.9	6.81	23.38

a larger semicircle at medium frequency (10 Hz–1 kHz) are observed. The smaller semicircle represents a charge-transfer resistance (R1) at the electrolyte/Pt counter electrode interface. The larger semicircle fits the recombination resistance (R2) at the TiO₂/dye/electrolyte interface [24, 25, 29]. For HTN samples, a small semicircle at lower frequency can also be observed obviously, which can be attributed to the diffusion resistance of redox species in the electrolyte [6]. Figure 7b shows the Bode EIS spectra of different photoanodes, based on it, the electron lifetime (τ_e) can be derived from the formula: $\tau_e = 1/2\pi f_{\max}$, where the f_{\max} is characteristic frequency of the maximum phase shift [24]. As shown in Table 2, all three HTN samples have smaller R2 than P25 electrode, which could be ascribed to the better electron transportation ability in 1D nanowires, and the HTN2 exhibits the smallest R2 value, it is reasonable that shorter growth time induces smaller nanowire diameter, and less defect in the nanowires, which will facilitate the electron transportation. It also imply that longer electron lifetime will be obtained due to less recombination traps in the thinner nanowires with shorter growth time, this can be confirmed by the longest electron lifetime of HTN2 among all four electrodes (Table 2). After

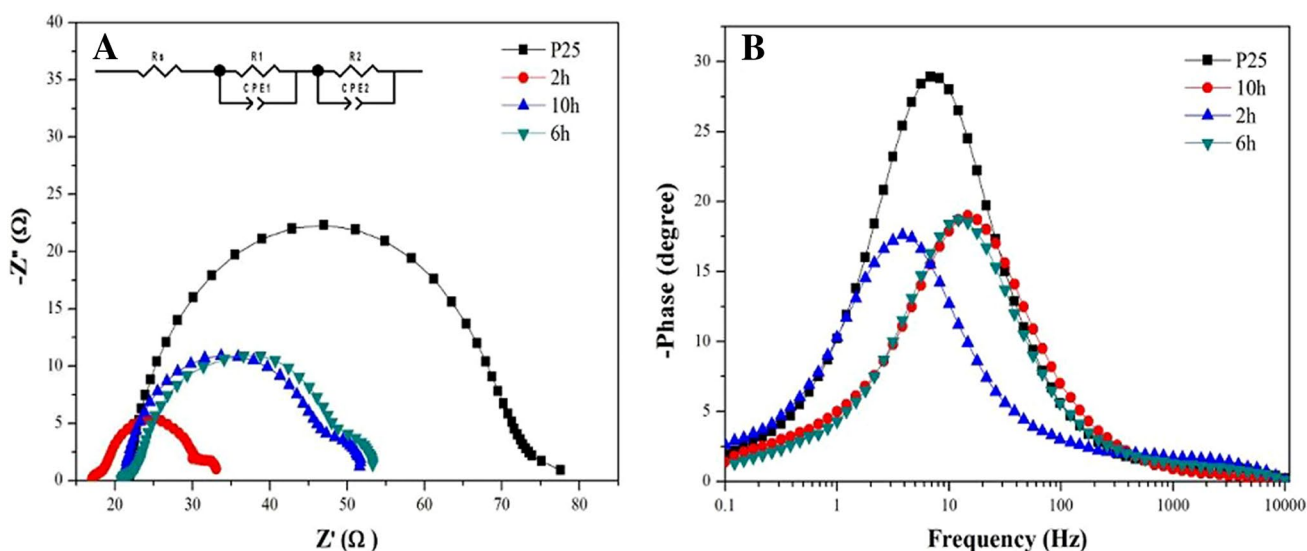


Fig. 7 a Nyquist plots and b Bode plots for photoanodes based on HTN2, HTN6, HTN10 and P25

longer reaction time (HTN6, HTN10), the electron lifetime decrease rapidly, and even is shorter than P25 electrode.

4 Conclusions

In summary, the hierarchical cotton-like TiO₂ nanomaterials constructed with nanowires are successfully synthesized at low temperature via a simple treatment of P25 in NaOH solution, and its size could be tuned by controlling the growth time, HTN consisting of untrathin (15 nm) nanowires could be obtained after 2 h growth, and it exhibits much improved DSSCs performance, a transform efficiency up to 8.9% could be obtained, which it is around 62% higher than untreated P25 photoanode. The excellent DSSCs performance of HTN could be attributed to the better dye adsorption ability induced by larger surface area and larger pore volume, and the better electron transportation ability along thinner 1D TiO₂ nanowires. The results provide the possibility to synthesize hierarchical TiO₂ nanomaterials with good performance via simple and low-cost process.

Acknowledgements This work was financially supported by the National Natural Science Foundation of China (Grant No. 51072124), the Program for New Century Excellent Talents in University (Grant No. NCET100605) and the Sichuan Science and Technology Program (Grant No. 2018GZ0463).

References

1. B. Oregan, M. Gratzel, *Nature* **353**, 737–740 (1991)
2. M. Grätzel, *Nature* **414**, 338–344 (2001)
3. M.-E. Yeoh, K.-Y. Chan, *Int. J. Energy Res.* **41**, 2446–2467 (2017)
4. X. Wang, Y. Wang, L. Yang, K. Wang, X. Lou, B. Cai, *J. Power Sources* **262**, 72–78 (2014)
5. X. Wang, Q. Meng, Y. Wang, H. Liang, Z. Bai, K. Wang, X. Lou, B. Cai, L. Yang, *Appl. Energy* **175**, 488–494 (2016)
6. S.P. Madhusudanan, B. Gangaja, A.G. Shyla, A.S. Nair, S.V. Nair, D. Santhanagopalan, *ACS Sustain. Chem. Eng.* **5**, 2393–2399 (2017)
7. K. Nakata, T. Ochiai, T. Murakami, A. Fujishima, *Electrochim. Acta* **84**, 103–111 (2012)
8. H. Hussain, G. Tocci, T. Woolcot, X. Torrelles, C.L. Pang, D.S. Humphrey, C.M. Yim, D.C. Grinter, G. Cabailh, O. Bikondoa, R. Lindsay, J. Zegenhagen, A. Michaelides, G. Thornton, *Nat. Mater.* **16**, 461–466 (2017)
9. Y. Lu, W.J. Yin, K.L. Peng, K. Wang, Q. Hu, A. Selloni, F.R. Chen, L.M. Liu, M.L. Sui, *Nat. Commun.* **9**, 2752 (2018)
10. M. Pelaez, N.T. Nolan, S.C. Pillai, M.K. Seery, P. Falaras, A.G. Kontos, P.S.M. Dunlop, J.W.J. Hamilton, J.A. Byrne, K. O’Shea, M.H. Entezari, D.D. Dionysiou, *Appl. Catal. B* **125**, 331–349 (2012)
11. W.Q. Wu, B.X. Lei, H.S. Rao, Y.F. Xu, Y.F. Wang, C.Y. Su, D.B. Kuang, *Sci. Rep.* **3**, 1352 (2013)
12. J.-Y. Liao, B.-X. Lei, H.-Y. Chen, D.-B. Kuang, C.-Y. Su, *Energy Environ. Sci.* **5**, 5750–5757 (2012)
13. X. Zhang, V. Thavasi, S.G. Mhaisalkar, S. Ramakrishna, *Nanoscale* **4**, 1707–1716 (2012)
14. P. Kartikay, S.S. Nemala, S. Mallick, *J. Mater. Sci.: Mater. Electron.* **28**, 11528–11533 (2017)
15. B. Liu, E.S. Aydil, *J. Am. Chem. Soc.* **131**, 3985–3990 (2009)
16. S.S. Mali, C.A. Betty, P.N. Bhosale, P.S. Patil, C.K. Hong, *Sci. Rep.* **4**, 5451 (2014)
17. Z. Seidalilir, R. Malekfar, H.P. Wu, J.W. Shiu, E.W. Diau, *ACS Appl. Mater. Interfaces* **7**, 12731–12739 (2015)
18. Z.-Y. Luo, D.-C. Mo, S.-S. Lu, *J. Mater. Sci.* **49**, 6742–6749 (2014)
19. K. Zhu, N.R. Neale, A. Miedaner, A.J. Frank, *Nano Lett.* **7**, 69–74 (2007)
20. M. Ye, X. Xin, C. Lin, Z. Lin, *Nano Lett.* **11**, 3214–3220 (2011)
21. H. Wang, B. Wang, J. Yu, Y. Hu, C. Xia, J. Zhang, R. Liu, *Sci. Rep.* **5**, 9305 (2015)
22. W.-Q. Wu, Y.-F. Xu, H.-S. Rao, C.-Y. Su, D.-B. Kuang, *Nanoscale* **5**, 4362–4369 (2013)
23. Y. Liu, R. Che, G. Chen, J. Fan, Z. Sun, Z. Wu, M. Wang, B. Li, J. Wei, Y. Wei, G. Wang, G. Guan, A.A. Elzatahry, A.A. Bagabas, A.M. Al-Enizi, Y. Deng, H. Peng, D. Zhao, *Sci. Adv.* **1**(4), e1500166 (2015)
24. J. Xiao, P. Li, X. Wen, *Nanotechnology* **29**, 175603 (2018)
25. G. Shang, J. Wu, M. Huang, Z. Lan, J. Lin, Q. Liu, M. Zheng, J. Huo, L. Liu, *J. Mater. Chem. A* **1**, 9869–9874 (2013)
26. T. Kasuga, M. Hiramatsu, A. Hoson, T. Sekino, K. Niihara, *Adv. Mater.* **11**, 1307–1311 (1999)
27. Y. Ohsaki, N. Masaki, T. Kitamura, Y. Wada, T. Okamoto, T. Sekino, K. Niihara, S. Yanagida, *Phys. Chem. Chem. Phys.* **7**, 4157–4163 (2005)
28. K.S.W. Sing, *Pure Appl. Chem.* **57**, 603–619 (1985)
29. Q. Zheng, H.S. Kang, J.J. Yun, J.Y. Lee, J.H. Park, S. Baik, *ACS Nano* **5**, 5088–5093 (2011)

Publisher’s Note Springer Nature remains neutral with regard to jurisdictional claims in published maps and institutional affiliations.